Vacuum 155 (2018) 612–618

Contents lists available at ScienceDirect

Vacuum

journal homepage: www.elsevier.com/locate/vacuum

Synthesis, structural and magnetic properties of $Co_{100-x}Pd_x$/GaAs thin films

A. Bourezg, A. Kharmouche*

Laboratory of Studies of Surfaces and Interfaces of Solid Materials (LESIMS), Ferhat ABBAS University Sétif1, Algeria

ARTICLE INFO

Keywords:
CoPd system
Thin films
Hysteresis curves
Coercivity
X-ray diffraction

ABSTRACT

Series of binary $Co_{100-x}Pd_x$ thin films are deposited onto GaAs (100) single-crystal semiconductor substrates by using thermal heating process under vacuum. The chemical compositions are analyzed by X-Ray Fluorescence technique, and the film morphologies are investigated by atomic force microscopy tools. The micro structural properties are studied using X-ray diffractometry. The static magnetic properties have been investigated by means of a vibrating sample magnetometer. The hysteresis loops display magnetization curves for ferromagnetic samples with the easy axis in the plane of the film. The coercive field ranges from 2 to 20 kA m^{-1} and decreases as a function of the grain size. The saturation magnetization decreases as the palladium content increases. Value of the squareness up to 98% has been found. These findings and others are analyzed and correlated.

1. Introduction

Magnetic thin films with perpendicular magnetic anisotropy have recently been investigated recently for the sake of applications in the field of magnetic recording media and magnetic random access memory devices [1–4]. It is well known that magnetic properties of ferromagnetic thin films are significantly affected by the methods and conditions of preparation and depend closely on the structural properties (crystallographic structure, texture, grain size and lattice constant). Co-based alloys usually present hard magnetic properties due to their highly anisotropic hexagonal close-packed (h.c.p.) crystalline structure. CoPd alloy films are attracting wide attentions for their applications in high-density magnetic and magneto-optical recording media, due to their strong perpendicular magnetic anisotropy and/or large Kerr rotation [5,6]. Not only CoPd thin films but also Co/Pd multilayers are known to be magnetically hard [7]. Hashimoto et al. [7] reported that 200 nm CoPd thick films, obtained by magnetron sputtering onto a glass substrate, display the same magnetic properties as the CoCr perpendicular magnetic recording material. In this case, the saturation magnetization M_s decreases monotonously with addition of Pd. Similar result was found by Kharmouche et al. with addition of Cr [8]. Their findings showed a magnetic easy axis normal to the film plane over the entire film thickness, a large coercivity H_c close to 1 kOe and a high remanence M_r. It is also reported that H_c and M_r/M_s increase with increasing Pd content. In the case of thin CoPd films, a high Kerr rotation and a perfect squareness of Kerr loop are obtained, indicating a possible use as magneto-optical recording media. Takata and Sumodjo reported that CoPd thin films, prepared by electrodeposition procedure with thickness ranging from 2.4 to 4.7 μm, were amorphous and the coercivity values ranged from 6.7 to 44.2 kA m^{-1}. The corresponding saturation magnetization, M_s, ranges from 0 to 1.73T, the magnetic easy axis being parallel to the film plane. It was also shown that H_c and M_s values increase and decrease, respectively, with increasing Pd content in CoPd alloys [9]. Gontarz et al. reported that $Co_{100-x}Pd_x$ alloys, electrodeposited from a single bath, display a strong perpendicular magnetic anisotropy in Pd-rich composition (x between 70 and 85 at. %) [10]. Ohtake et al. found that CoPd thin films of 40 nm thickness, deposited on MgO (111) substrate by radio frequency (rf) magnetron sputtering at temperature ranging from RT to 600 °C, grow epitaxially at temperatures higher than 200 °C. Below this temperature, the obtained CoPd films are amorphous [2]. Yabuhara et al. prepared CoPd alloy thin films on MgO single-crystal substrates of $(001)_{B1}$, $(110)_{B1}$, and $(111)_{B1}$ orientations at 600 °C by ultra high vacuum rf magnetron sputtering. They obtained a perpendicular magnetic anisotropy and reported that A1- CoPd (001), (110) and (111) films are respectively formed on MgO $(001)_{B1}$, $(110)_{B1}$, and $(111)_{B1}$ substrates. However, L_{10} ordered CoPd structure has not been obtained. Magnetic properties of these films are considered to be reflecting the magnetocrystalline anisotropy of bulk A1 and L_{10} crystals [11]. Nozawa et al. prepared CoM (M = Pt, Pd, Rh) disordered films by direct-current magnetron sputtering under an Ar gas pressure of 0.6 Pa on 2.5 inch glass substrates at RT. They showed that M_s gradually decreased with increasing Pd and Rh content, and reported that $Co_{50}Rh_{50}$ film has nearly perfect h. c.p. stacking faults in h. c.p. grains, while the $Co_{50}Pt_{50}$ and $Co_{50}Pd_{50}$ films contain SFs. When substituting Pt by Rh the coercivity was found to be 10 times larger than that for the $Co_{50}Pt_{50}$ film [12]. Myagkov et al.

* Corresponding author.
E-mail addresses: kharmouche_ahmed@yahoo.fr, kharmouche_ahmed@univ-setif.dz (A. Kharmouche).

https://doi.org/10.1016/j.vacuum.2018.06.062
Received 29 May 2018; Received in revised form 20 June 2018; Accepted 26 June 2018
Available online 28 June 2018
0042-207X/

prepared films by sequential vacuum of polycrystalline Pd/Co bilayers. They evidenced that the solid-state reaction between the Co and the Pd films begin to occur at temperature T = 400 °C and is fully completed at 650 °C with the formation of CoPd phase [13]. Gan'shina et al. observed relatively higher values of coercivity (33.5–52.6 kA m^{-1}) for Pd-rich CoPd alloys with perpendicular magnetic anisotropy [14]. Hu et al. reported that Co_xPd_{1-x} nanowire arrays obtained by electrodeposition technique, display the highest coercivity of 90 kA m^{-1} and the best squareness of 94%, corresponding to an optimum composition of $Co_{0.73}Pd_{0.27}$ at 300 K [15]. Vivas et al. reported that granular CoPd alloyed and assembled nanoparticles, prepared by room temperature sequential sputtering deposition on amorphous alumina, showed perpendicular magnetic anisotropy and evidenced three magnetic phases: hard-ferro, soft-ferro and superparamagnetism [16]. Maximenko and co-authors presented a systematic analysis of magnetization curves which evidenced perpendicular magnetic anisotropy of CoPd antidot arrays, while FePd antidot arrays revealed isotropic magnetic anisotropy. Their results also indicated an increased out-of-plane magnetic contribution and, at the same time, an ordered $L1_0$ structure was obtained under successive vacuum annealing at 530 °C elevated temperatures [17]. Hsu et al. reported an evolution of morphology and magnetism in Co-Pd alloy films where nanoclusters were composed of Co-oxide with an underneath Pd-rich alloy layer. With Co-oxide nanoclusters, they remarked that magnetic easy axis was altered to in-plane direction [18]. Flat-surface Al_2O_3 templates were used for the first time by T.N. Anh Nguyen et al. for fabrication of Co/Pd and Co/Pt porous films with strong perpendicular magnetic anisotropy [19]. Flattened morphology of porous films favors their perfect out-of-plane anisotropy. H-J Anklam et al. used dc magnetron sputtering technique to deposit single layers of CoCr onto Si substrate and report excellent magnetic and morphological properties [20]. Using Auger electron spectroscopy and thermal desorption spectroscopy, M. Krawczyk reports an interesting study on the interaction of O_2 with polycrystalline $Co_{50}Pd_{50}$ alloy samples oxidized in the temperature range of 300–773K with oxygen exposure up to 405 L [21]. Sheng-Chi Chen and Ta-Huang Sun used rapid thermal annealing to fabricate granular L10 FePt nanocomposite on natural-oxidized Si (100) substrate. They report in-plane and perpendicular coercivities of FePt films equal to 513 and 430 kA/m, respectively [22]. Andreas Kaidatzis et al. used magnetron sputtering to produce ultrathin FePt on monocrystalline MgO < 001 > substrates at 500 °C. They report $L1_0$ structure and perpendicular magnetic anisotropy for films thicker than 2.7 nm with an out-of-plane coercivity as high as 16 kOe, whereas for thinner films (down to 1 nm) an in-plane-anisotropy occurs with a coercivity dropping to 0.5 kOe [23]. G. Varvaro et al. reported a very interesting study with regard to the single phase $L1_0$ FePt films. Due to its elevated magneto-crystalline anisotropy, up to 10 MJ/m^3, which allows it to remain thermally stable still when the grain sizes are lower than 3 nm, this alloy is considered among the most promising magnetic materials, candidates for recording media [24].

In this work, we study the structural, morphological and magnetic properties of $Co_{100-x}Pd_x$ thin films, synthesized by thermal evaporation process under vacuum. These properties are studied as a function of palladium content.

2. Material and methods

We have evaporated under vacuum, $Co_{100-x}Pd_x$ thin films, typically 150 nm in thickness, onto GaAs semiconductor substrate. The mixture is issued from a 99.99% pure Co and Pd powders, provided by Goodfellow SARL. The vacuum system consists of a primary pump, and a secondary oil diffusion pump cooled by a constant and continuous circulation of water in a coil. All the stages of deposition were done at room temperature. The atomic vapor flow leaves the crucible made of tungsten and reaches the substrates under a perpendicular incidence. Prior to the deposition, the pressure in the compartment was 133×10^{-7} Pa; throughout the evaporation, the base pressure was lower than 133×10^{-6} Pa. The deposition rate has been kept equal to 0.2 nm per second, i.e., 12 nm per minute. The thickness of the samples were measured using a Veeco Dektak 150 profilometer and the chemical composition was analyzed by XRF (X-Ray Fluorescence) technique, using ZSX Primus IV Rigaku, working at the temperature of 36.50 °C and the pressure 2.9 Pa. The average current was fixed at 100 mA and the tension at 50 kV. P-10 Gas (10%Methane + 90%Argon) has been used for the detector. The tube temperature was kept at 20 °C, the used fluorescence energy being 6.4 keV FeKα, and 6.9 keV CoKα. The structural properties were studied using a Siemens D500 X-ray diffractometer working in the 2θ mode of the Bragg-Brentano geometry, with the Cu Kα radiation wavelength (λ = 0.15406 nm). The diffractometer is equipped with Ni filter and operates at 35 kV and 30 mA. The scattering angle has been chosen to range from 20 to 100°, with a step of 0.02°. The counting time has been settled to 0.2 s per step. The X-ray diffraction patterns analyses were performed with X'Pert High Score software. The hysteresis loops were obtained by means of a MicroSense EZ7 Vibrating Sample Magnetometer (VSM), working at ambient temperature, and providing magnetic field intensity up to 2 T. The low field noise is less than 5×10^{-7} T and the sensibility is below 0.5×10^{-9} A m^2. The film morphologies and surface states were observed using a Veeco 3100 atomic force microscope (AFM), with no-contact mode, at room temperature. The scanning speed used is 1 Hz.

3. Results and discussion

3.1. Atomic composition

Table 1 displays the atomic composition of the evaporated $Co_{100-x}Pd_x$ samples. These values of Pd content range from 8 to 31 at. % and play a crucial role on the main magnetic properties of these thin films, as will be revealed subsequently.

3.2. Structural study

X-Ray diffraction measurements have been performed to study the crystal structure and microstructure of the $Co_{100-x}Pd_x$ samples. For the purpose, selected X-ray diffraction patterns for the $Co_{100-x}Pd_x$/GaAs thin films are shown in Fig. 1. Here, the contribution of $K\alpha_2$ line has been analytically stripped from all profiles. Besides the diffraction peaks related to the GaAs substrate, not shown here for sake of brevity, the X-ray scans shown in Fig. 1 display two Bragg peaks which correspond to the diffraction planes related to CoPd material in the face centered cubic (f.c.c.) structure, with Miller indices (220) and hexagonal close packed (h.c.p.) Co(422), according to the PDF (powder diffraction file) cards [25,26]. Using these peaks, the lattice parameters have then been derived from the X-ray spectra.

To compare these lattice parameters to the bulk CoPd ones, one may

Table 1
Atomic composition of $Co_{100-x}Pd_x$ samples, lattice parameter *a*, grain size L, microstrain ε, root mean square roughness (rms) and coercive field H_c as a function of palladium content.

Pd (at.%)	8	9	20	28	31
a (nm)	0.371	0.370	0.370	0.370	0.375
L (nm)	4.8	17.1	10.7	11.4	21.6
ε(%)	3.21	2.85	3.51	2.72	3.28
rms roughness (nm)	8.4	1	1.5	1.1	0.7
H_c (kA.m^{-1})	20	2	46	3.20	1.76

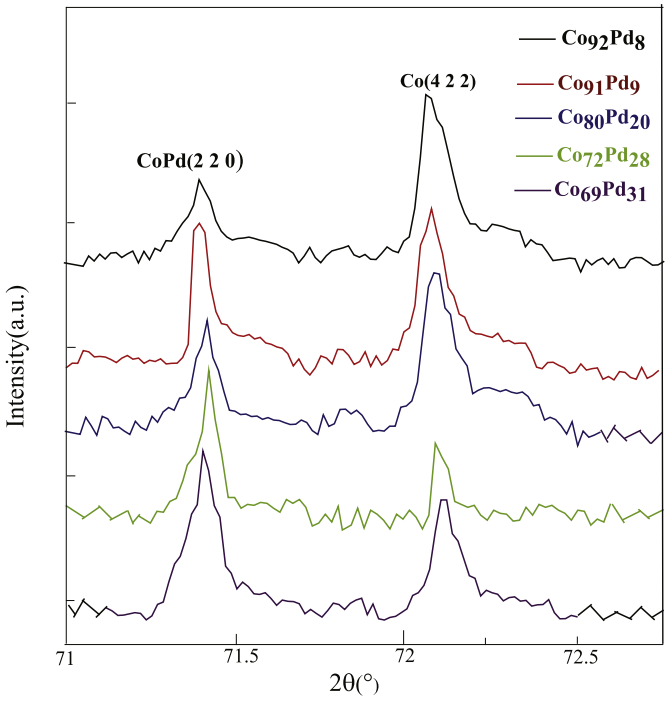

Fig. 1. Selected X-ray diffraction patterns for the $Co_{100-x}Pd_x$/GaAs thin films.

have access to the bulk value of the parameter *a*, with the help of the lattice spacing $d_{(220)}$ values provided by Tobari et al. [27] using RHEED and XRD measurements. The measured value is $d_{(220)\ bulk} = 0.133$ nm.

For the cubic system

$$a = d\sqrt{h^2 + k^2 + l^2} \tag{1}$$

Using the Miller indices values in the present diffraction spectra, we deduce

$$a_{bulk\,(220)} = d_{bulk\,(220)} \times \sqrt{8} \tag{2}$$

We found $a = 0.376$ nm.

This value is greater than those displayed in Table 1. We conclude therefore that all the samples are under a tensile stress.

Furthermore, we have also computed the crystallite size using the X-ray diffraction patterns and the Scherer formula:

$$L = \frac{k\,\lambda}{\Delta(2\theta)cos\theta} \tag{3}$$

where L is the grain size for a grain with a particular orientation, k a dimensionless integer sensibly equals to 1, λ the X-ray wave length, θ the diffraction angle and Δθ the full width at half height of the Bragg peak corresponding to this particular orientation [28]. The micro strains were computed by using the Stokes-Wilson formula:

$$\varepsilon = \frac{\beta}{4tan\theta} \tag{4}$$

β being the integral width corresponding to the given orientation and θ, the diffraction angle [29]. From Table 1, it is clear that neither the evolution of the crystallite size L nor the variation of the microstrain ε with the palladium content presents any noticeable feature. The values of L are ranging from 10.7 to 13.8 nm as the palladium content fluctuates between 8 and 31 at.%, for (220) Bragg diffraction peak. At the same time, the values of ε are restricted between 2.72 and 3.51% for (220) Bragg peak, as clearly shown in Table 1. On the contrary, the evolution of the microstrain with the crystallite size displays an

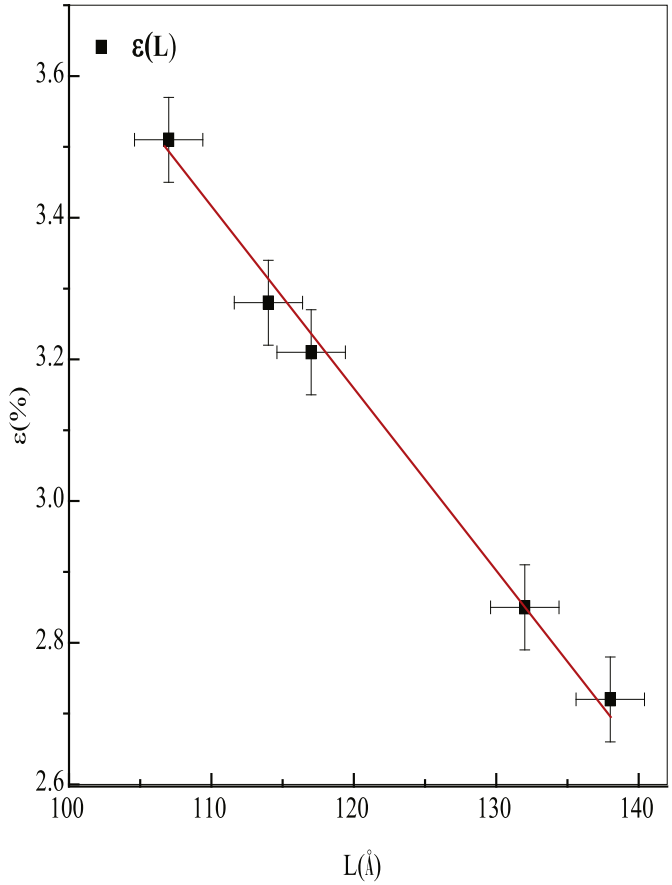

Fig. 2. Microstrain as a function of crystallite size. The bold points are experimental values; the straight line is just a guide for the eyes.

interesting aspect as depicted in Fig. 2. Undeniably, the microstrain decreases as the crystallite size increases. Indeed, as the crystallite size grows, the layers are lesser under stress, and the cell parameter tends to its natural length which minimizes the difference between the measured parameter of the thin film *a* and the value of the bulk parameter; therefore, the microstrain diminishes. On another hand, topographic images recorded by the atomic force microscope are presented in Fig. 3. It is well known that magnetic properties of thin films depend closely on surface/interface roughness. The surface roughness influences mainly the coercivity and the magnetic anisotropy [30,31]. Roughness affects the motion of the domains walls for each type of wall. It causes an increase in the coercivity due to the rotation of the domains for the Néel walls and a decrease of the same coercivity for the Bloch walls. This property was confirmed by Zhao et al. [32], Li. et al. [33,34] and Malyutin et al. [35]. The specimen of AFM scans presented in Fig. 3 reveal smooth surfaces for several films, the root mean square (rms) roughness amplitude being as small as 0.7 nm for the smoothest film corresponding to $Co_{69}Pd_{31}$ sample.

3.3. Magnetic study

3.3.1. Saturation magnetization

Pure Pd has no spontaneous magnetization whereas bulk Co has a saturation magnetization equal to 1.78 T [36]. The magnetization curves of our evaporated CoPd thin films have been recorded by means of VSM tools. Representative hysteresis curves are shown in Fig. 4. These loops are obtained for the longitudinal configuration, explicitly,

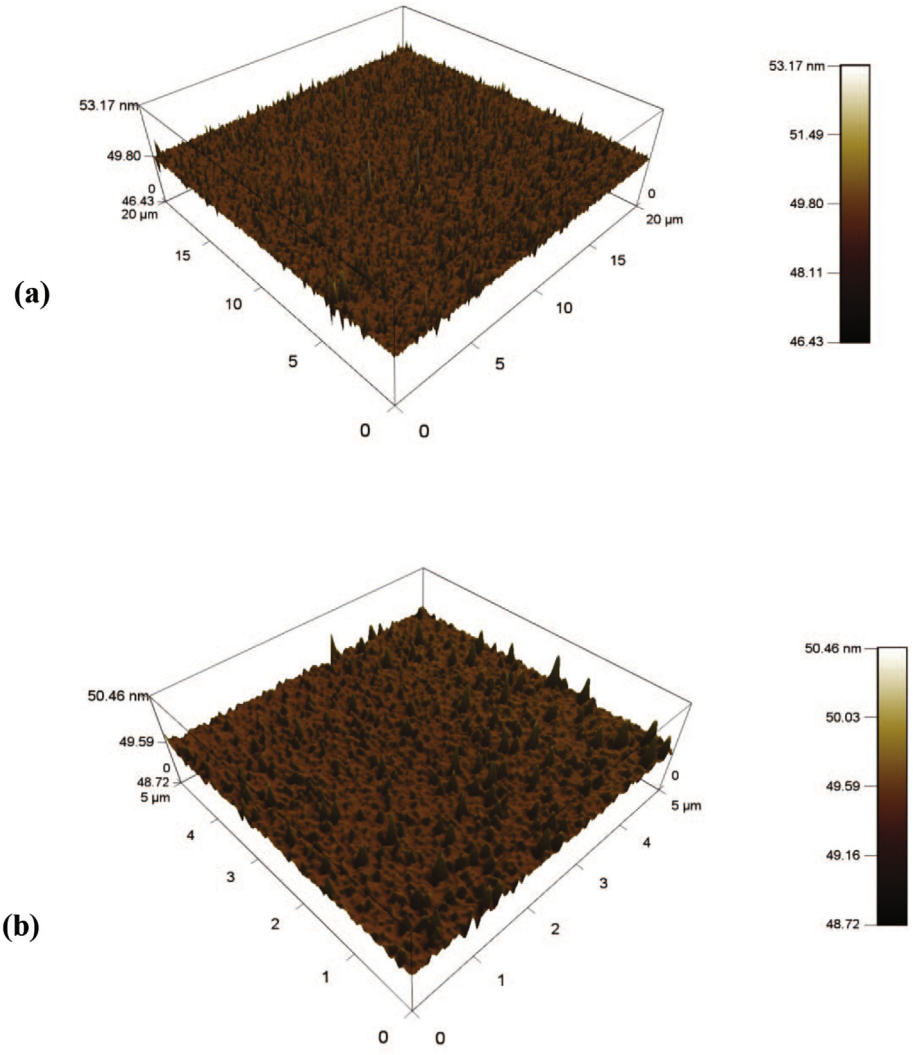

Fig. 3. AFM topographic surface images for $Co_{80}Pd_{20}$ thin film; scan areas 20 µm × 20 µm (a), 5 µm × 5 µm (b).

the arrangement where the external magnetic field H is applied parallel to the film plane. For the polar configuration (not shown here) where the external magnetic field H is applied perpendicular to the film plane, the saturation magnetization is reached only after applying a relatively large magnetic field. From the shape of the hysteresis loops it appears that the easy magnetization axis lies in the film plane, with no preferential in-plane orientation, for all the thin films considered. Several parameters, such as the coercive field H_c, the magnetic moment m, the saturation magnetization M_s, and the remnant magnetization M_r, are extracted from the hysteresis loops. Fig. 5 displays the evolution of the saturation magnetization M_s as a function of palladium content. On this figure we remark clearly that M_s values decrease gradually from 1.445T for $Co_{92}Pd_8$ to 0.238 T for $Co_{69}Pd_{31}$ thin films. This progressive decrease of the spontaneous magnetization is due to the fact that Pd atoms are polarized and their moments are parallel to the Co moments [37,38]. It is worth noting that M_s evolution as a function of Pd content, compared to the same evolution versus Cr content, shows that this latter decreases quicker. This trend is a consequence of the fact that the Cr moments are aligned antiparallel to Co moment as reported in previous works [39]; similar trend has been reported by other authors [12] [39,40]. Moreover, in Fig. 4, the hysteresis loop shape suggests that squareness has been improved as the Pd content increases. Let us recall that Co thin films mostly crystallize in hexagonal close packed (h.c.p) structure [41–47]. This h.c.p. phase enhances the competition between the crystalline and the shape anisotropies and therefore decreases the squareness [9]. When the Pd content increases in the CoPd alloy, f.c.c. phase appears, not present in our work, which reduces the competition between the crystalline and the shape anisotropies and therefore enhances the squareness.

3.3.2. Coercivity

Fig. 6 displays the variations of the coercive field H_c as a function of the crystallite size. L is the length equal to the sum of the distances between all the diffracting planes. It is significant to notice that H_c values fluctuate between 20 kA m^{-1} for L equal to 4.8 nm, and 1.76 kA m^{-1} for L equal to 21.6 nm. The highest value of coercivity, 20 kA m^{-1}, corresponding to the lowest value of crystallite size, 4.8 nm, is probably due to the relatively great number of ground boundaries present in the thin layer. Large crystallite size provides low coercive field values and vice versa. Therefore, the coercivity in our films may be probably related with domain wall motion across grain boundaries. Moreover, coercivity is also affected by surface roughness. Because of

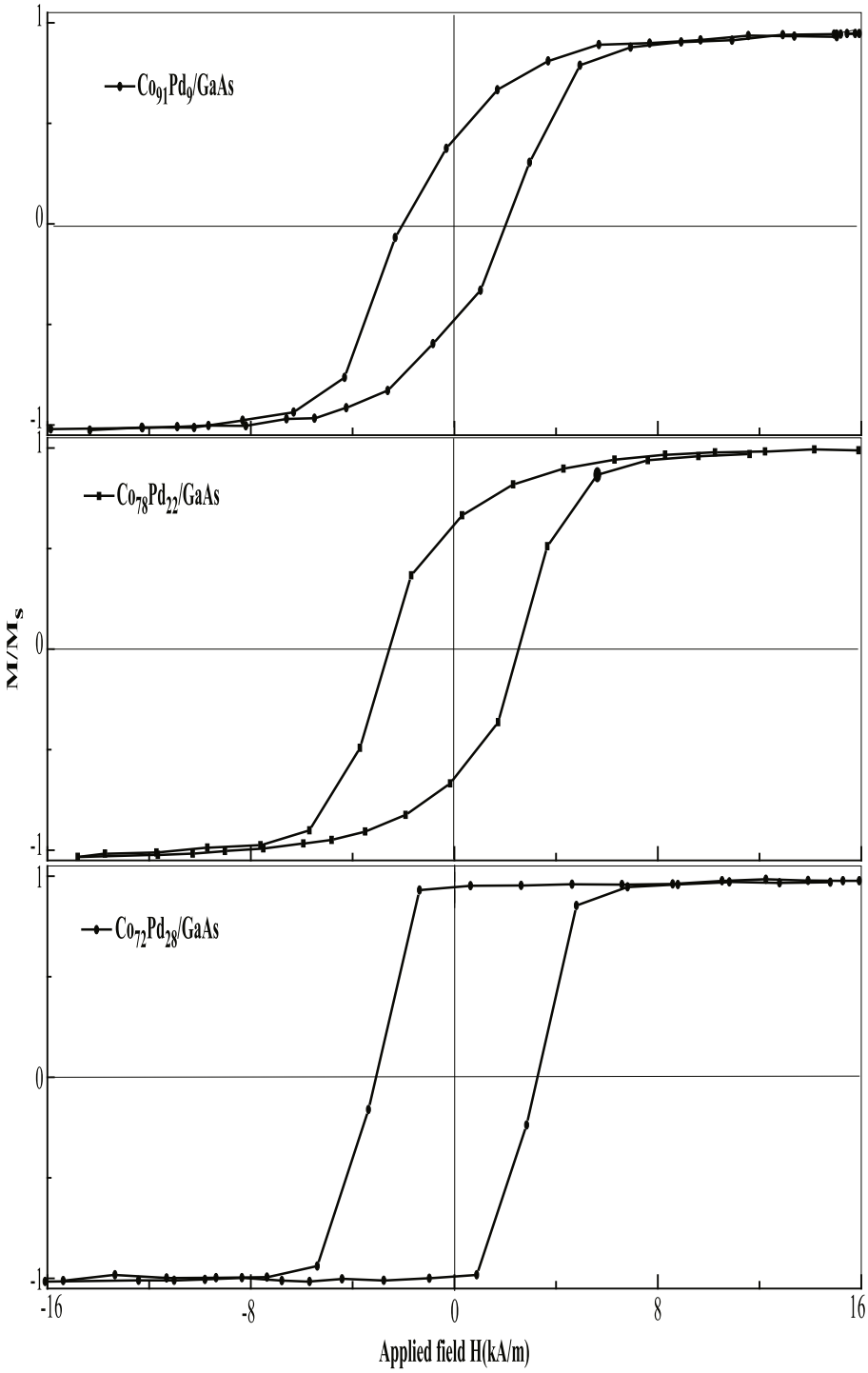

Fig. 4. Representative Hysteresis curves for the $Co_{100-x}Pd_x$/GaAs thin films, recorded in the longitudinal configuration. Indications are inside the figure.

the presence of pinning centers in the magnetic domain walls in the rough film, the surface roughness makes the demagnetizing factors non null along the planar directions of the thin layer, and therefore, affects the movement of the domain [48,49]. As already pointed out in Section 3.2, surface roughness induces an enhancement in the coercivity due to the rotation of the domains for the Néel walls and a reduction of the same coercivity for the Bloch walls [30,31]. The influence of the surface roughness on the coercivity is illustrated in Fig. 7. This latter clearly shows an increase of the coercive field, from 1.76 kA m^{-1}, for rms roughness value equal to 0.7 nm, to 20 kA m^{-1}, for 8.4 nm as rms roughness value. The smallest value of rms roughness is related to the lowest value of H_c and the greatest value of rms roughness is associated to the highest value of H_c. This indicates undoubtedly the correlation between surface roughness and coercivity for these $Co_{100-x}Pd_x$ thin films deposited onto GaAs(100).

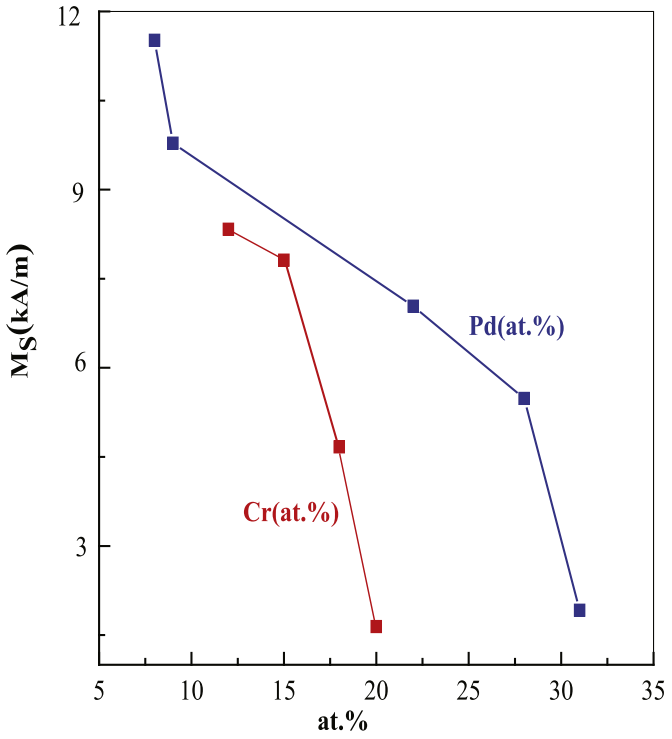

Fig. 5. Saturation magnetization M_s versus palladium and chromium content for $Co_{100-x}Pd_x$ and $Co_{100-x}Cr_x$; the points are experimental data and the straight lines are just guide for the eyes.

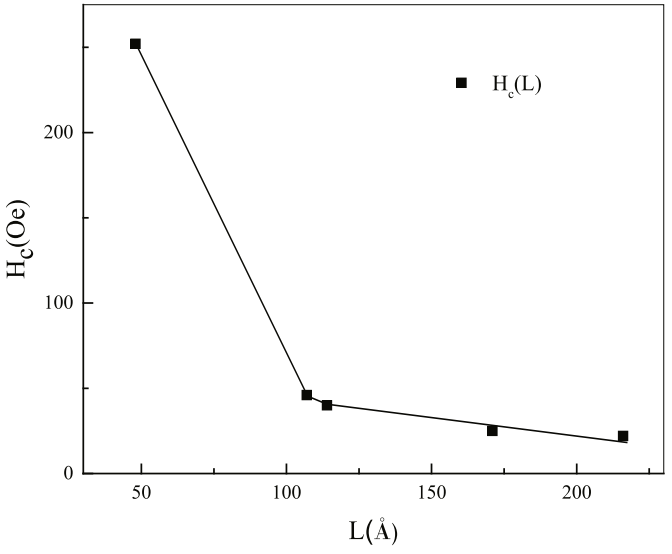

Fig. 6. Variations of the coercive field H_c as a function of the crystallite size L.

4. Conclusion

The magnetic and structural properties of $Co_{100-x}Pd_x$ thin films, prepared by evaporation under vacuum on GaAs substrate, have been studied as a function of Pd content. X ray diffraction studies infer that the films are polycrystalline and show a face centered cubic structure. All the samples are under stress. VSM measurements conclude to an in plane magnetization with no preferential orientation, and a saturation magnetization decreasing with increasing Pd content, from 1.445 T for $Co_{92}Pd_8$ to 0.238 T for $Co_{69}Pd_{31}$. Values of squareness up to 98% have been measured. The coercivity in our $Co_{100-x}Pd_x$ thin films may probably be related to domain wall motion across grain boundaries.

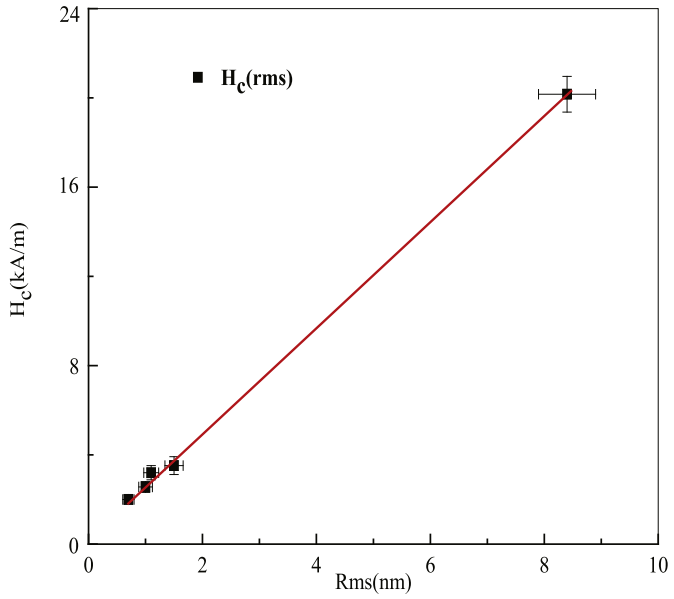

Fig. 7. Variations of the coercive field H_c as a function of the root mean square roughness (rms).

Acknowledgments

The authors warmly thank the Director of the URME of Sétif1 University, Prof. Mohamed HAMIDOUCHE and his team, as well as the Director of LCIMN laboratory, Prof. Amor AZIZI and his team, for alloying Mrs. Ahlem BOUREZG to carry out several experiments within their respective laboratories.

References

[1] Osamu Yabuhara, Mitsuru Ohtake, Kouske Tobari, Tsutomu Nishiyama, Fumiyoshi Kirino, Masaaki Futamoto, Thin Solid Films 519 (2011) 8359–8362.
[2] Mitsuru Ohtake, Shouhei Ouchi, Fumiyoshi Kirino, Masaaki Futamoto, IEEE Trans. Magnesium 48 (2012) 3595–3598.
[3] P.R. Aitchison, J.N. Chapman, V. Gehanno, I.S. Weir, M.R. Scheinfein, S. McVitie, A. Marty, J. Magn. Magn Mater. 223 (2001) 138–146.
[4] Zoë Kugler, Volker Drewello, Markus Schäfers, Jan Schmalhorst, Günter Reiss, Andy Thomas, J. Magn. Magn Mater. 323 (2011) 198–201.
[5] J.R. Childress, J.L. Duvail, S. Jasmin, A. Barthélémy, A. Fert, A. Schuhl, O. Durand, P. Galtier, J. Appl. Phys. 75 (1994) 6412.
[6] S.U. Jen, C.M. Chung, W.L. Chen, J. Magn. Magn Mater. 220 (2000) 205–213.
[7] S. Hashimoto, Y. Ochiai, K. Aso, Jpn. J. Appl. Phys. 28 (1989) 1596–1599.
[8] A. Kharmouche, S.M. Cherif, G. Schmerber, A. Bourzami, J. Magn. Magn Mater. 310 (2007) 152–158.
[9] F.M. Takata, P.T.A. Sumodjo, J. Electroch. Acta 52 (2007) 6089–6096.
[10] R. Gontarz, L. Smardz, B. Szymanski, P. Juzikis, J. Magn. Magn Mater. 120 (1993) 278–280.
[11] Osamu Yabuhara, Mitsuru Ohtake, Kouske Tobari, Tsutomu Nishiyama, Fumiyoshi Kirino, Masaaki Futamoto, Thin Solid Films 519 (2011) 8359–8362.
[12] Naoki Nozawa, Shin Saito, Shintaro Hinata, Migaku Takahashi, J. Phys. D Appl. Phys. 46 (2013) 172001.
[13] V.G. Myagkov, L.E. Bykova, V.S. Zhigalov, I.A. Tambasov, G.N. Bondarenko, A.A. Matsinin, N. Rybakova, Phys. Solid State 57 (2015) 1014–1022.
[14] E. Gan'shina, V. Guschin, I. Romanov, A. Skobelev, A. Tselev, J. Magn, Magn. Mater 185 (1998) 258–364.
[15] H.N. Hu, H.Y. Chen, S.Y. Yu, L.J. Chen, J.L. Chen, G.H. Wu, J. Magn. Magn Mater. 299 (2006) 170–175.
[16] L.G. Vivas, A.I. Figueroa, F. Bartolomé, J. Rubín, L.M. García, C. Deranlot, F. Petroff, L. Ruiz, J.M. González-Calbet, N.B. Brookes, F. Wilhelm, A. Rogalev, J. Bartolomé, J. Magn. Magn. Mater 400 (2016) 248–252.
[17] A. Maximenko, J. Fedotova, M. Marszałek, A. Zarzycki, Y. Zabila, J. Magn. Magn Mater. 400 (2016) 200–205.
[18] Chuan-Che Hsu, Hsiang-Chih Chiu, Venkata Ramana Mudinepalli, Yu-Chuan Chen, Po-Chun Chang, Chun-Te Wu, Hung-Wei Yen, Wen-Chin Lin, Appl. Surf. Sci. 416 (2017) 133–143.
[19] T.N. Anh Nguyen, J. Fedotova, J. Kasiuk, V. Bayev, O. Kupreeva, S. Lazarouk, D.H. Manh, D.L. Vu, S. Chung, J. Åkerman, V. Altynov, A. Maximenko, Appl. Surf. Sci. 427 (2018) 649–655.
[20] H.-J. Anklam, L. Fritzsch, R. Mattheis, S. Müller-Pfeiffer, F. Thrum, Vacuum 40 (1990) 513–515.

[21] M. Krawczyk, Vacuum 63 (2001) 23–27.
[22] Sheng-Chi Chen, Ta-Huang Sun, Vacuum 84 (2010) 1430–1434.
[23] Andreas Kaidatzis, Vassilis Psycharis, Georgios Giannopoulos, José Miguel García-Martín, Dimitrios Niarchos, Phys. Status Solidi RRL 1–4 (2016), http://dx.doi.org/10.1002/pssr.201600386.
[24] G. Varvaro, S. Laureti, D. Fiorani, J. Magn. Magn Mater. 368 (2014) 415–420, http://dx.doi.org/10.1016/j.jmmm.2014.04.058.
[25] JCPDF 03-065-6075, Calculated from NIST using POWD-12++, Matsuo, Y., J. Phys. Soc. Jpn., 32, 972, (1972).
[26] JCPDF 03-065-9722, Calculated from NIST using POWD-12++, Krainer, E., Robitsch, J., Z. Metallkd., 61, 350, (1970).
[27] Kousuke Tobari, Mitsuru Ohtake, Katsumasa Nagano, Masaaki Futamoto, Jpn. J. Appl. Phys. 50 (2011) 073001.
[28] J.P. Eberhart, Analyse Structurale et Chimiques des Matériaux, Bordas, Paris, 1998.
[29] D. Louër, Journal de Physique IV Fr 103 (2003) 321.
[30] J.A.C. Bland, B. Heinrich (Eds.), Ultrathin Magnetic Structure I and II, Springer-Verlag, Berlin, Germany, 1994.
[31] P. Bruno, G. Bayureuther, P. Beauvillain, C. Chappert, G. Luger, D. Renard, J.P. Renard, J. Seiden, J. Appl. Phys. 68 (1998) 5759.
[32] Y.-P. Zhao, R.M. Gamache, G.-C. Wang, T.-M. Lu, G. Palasabtzas, J.Th M. De Hosson, J. Appl. Phys. 89 (2001) 1325.
[33] M. Li, G.-C. Wang, H.-G. Min, J. Appl. Phys. 83 (1998) 5313.
[34] M. Li, Y.-P. Zhao, G.-C. Wang, H.-G. Min, J. Appl. Phys. 83 (1998) 6287.
[35] V.I. Malyutin, V.E. Osukhovskii, Yu D. Vorobiev, A.G. Shishkov, V.V. Yudin, Phys. Status Solidi 65 (1981) 45.
[36] American Institute of Physics Handbook, second ed., Mc-Graw-Hill, New York, 1963.
[37] R.M. Bozorth, P.A. Wolff, D.D. Davis, V.B. Compton, J.H. Wernick, Phys. Rev. 122 (1961) 1157.
[38] O. Rader, E. Vescovo, J. Redinger, S. Blügel, C. Carbone, W. Eberhardt, W. Gudat, Phys. Rev. Lett. 72 (1994) 2247–2251.
[39] J. Carrey, A.E. Berkowitz, W.F. Egelhoff Jr., D.J. Smith, Appl. Phys. Lett. 83 (2003) 5259.
[40] A. Kharmouche, S.-M. Chérif, Y. Roussigné, G. Schmerber, Appl. Surf. Sci. 255 (2009) 6173–6178.
[41] Subhradip Ghosh, Chhanda Basu Chaudhuri, Biplab Sanyal, Abhijit Mookerjee, J. Magn. Magn Mater. 234 (2001) 100–113.
[42] Hashimoto Shunichi, Ochiai Yoshitaka, Aso Koichi, Jpn. J. Appl. Phys. 28 (1989) 1596–1599.
[43] G. Zangari, B. Bozzini, P.L. Cavallotti, G. Fontana, P.G. Maisto, E. Terrenzio, J. Magn. Magn Mater. 133 (1994) 511–515.
[44] A. Kharmouche, J.Nanosci. Nanotechnology 11 (2011) 4757–4764.
[45] A. Kharmouche, S.-M. Chérif, A. Bourzami, A. Layadi, G. Schmerber, J. Phys. D Appl. Phys. 37 (2004) 2583–2587.
[46] A. Kharmouche, J. Ben Youssef, A. Layadi, S.-M. Chérif, J. Appl. Phys. 101 (2007) 113910.
[47] A. Kharmouche, J. Supercond. Nov. Magnetism 30 (2017) 3295–3299.
[48] Y.-P. Zhao, R.M. Gamache, G.-C. Wang, T.-M. Lu, G. Palasantzas, J.ThM. De Hosson, J. Appl. Phys. 89 (2001) 1325.
[49] Q. Jiang, H.-N. Yang, G.-C. Wang, Surf. Sci. 373 (1997) 181.